

# COMPARISON OF MACHINE LEARNING ALGORITHMS FOR LAND USE AND LAND COVER ANALYSIS USING GOOGLE EARTH ENGINE (CASE STUDY: WANGGU WATERSHED)

Septianto Aldiansyah<sup>1</sup>, Randi Adrian Saputra<sup>2</sup>

<sup>1</sup>Department of Geography, Faculty of Mathematics and Natural Sciences, Universitas Indonesia

<sup>2</sup>Department of Geography Education, Faculty of Teacher Training and Education, Universitas Halu Oleo

\*e-mail: septiantoaldiansyah863@gmail.com

Received:27.10.2022; Revised:31.12.2022; Approved: 31.12.2022

**Abstract.** Human population growth and land use and land cover (LULC) change have always developed side by side. Considering selection of a good Machine Learning (ML) classifier algorithm is needed considering the high estimation of LULC maps based on remote sensing. This study aims to produce a LULC classification of Landsat-8 and Sentinel-2 images by comparing the accuracy performance of three ML algorithms, namely: Classification and Regression Tree (CART), Random Forest (RF), and Support Vector Machine (SVM). Dataset comparison ratios were also explored to find the LULC classification results with the best accuracy. Sentinel-2 is better than Landsat-8 regarding Overall Accuracy (OA) and Coefficient Kappa. The comparison ratio of the training and testing datasets with a good level of accuracy is 70:30 on both images with the average OA Landsat-8 and Sentinel-2 being 92.09% and 94.21%, respectively. The RF algorithm outperforms CART and SVM in both types of satellite imagery. The mean OA of the CART, RF, and SVM classifiers was 92.03%, 94.74%, 83.54% on Landsat-8, 93.14%, 96.15%, and 93.34% on Sentinel-2, respectively.

**Keywords:** *Google Earth Engine; Land Use Land Cover; Classification and Regression Tree; Random Forest; Support Vector Machine*

## 1 INTRODUCTION

Future studies will be easier to understand by understanding Land Use and Land Cover (LULC) forms of various scales for various global phenomena such as drought, flooding, erosion, migration, and climate change. Continuous and accurate LULC analysis is an integral part of sustainable development activities carried out in certain areas. LULC maps become an important component for various scientific studies involving the effects of climate change on river flows and watersheds (Sridhar et al., 2019), geomorphology (Sujatha & Sridhar, 2018), groundwater management (Sridhar et al., 2018; Xiao et al., 2021; Xiao et al., 2021; Xiao et al., 2022), social knowledge for natural resource management (Sridhar et al., 2021), and monitoring agricultural land (Sridhar et al., 2017; Jamali et al., 2019; Rahman et al., 2020). A land can use the LULC map in determining suitable land for

agricultural activities so that watershed management can be more sustainable (Cihlar, 2000, Renschler & Harbor, 2002).

Remote sensing is the most commonly used method of mapping land cover and tracking its changes over time (Phan et al., 2020). With an increasing population and the need to develop new areas to meet the demand for food production, energy generation, and water security, the hydrological and water resource modeling community is interested in integrating and evaluating land use changes and their effects on watershed areas (Kang et al., 2019; Setti et al., 2020).

Limitations in making low-resolution land cover maps in a wide area of course involve large amounts of data. Hefty storage capacity, processing power, and flexibility are required to implement a diversified approach (Xie et al., 2019). This problem has been addressed by the new Google Earth Engine (GEE)

technology. GEE is a form of integration of remote sensing and big data into a high-performance cloud-based platform and enables fast and easy computing of satellite imagery (Gorelick et al., 2017; Sidhu et al., 2018; Tamiminia et al., 2020; Kolli et al., 2020; Aldiansyah et al., 2021; Rahmi et al., 2022).

The GEE platform provides independent satellite imagery of various spatial resolutions. The platform is built in JavaScript and Python in handling coding (Shelestov et al., 2017; Mateo-García et al., 2018; Pimple et al., 2018) using MapReduce architecture for parallel processing which is a technique for breaking large amounts of data into small parts and processing them across multiple devices. LULC classification results using non-parametric Machine Learning (ML) methods such as Classification and Regression Trees (CART), Support Vector Machine (SVM), and Random Forest (RF) have very accurate accuracy (Bar et al., 2020; Liu et al., 2020; Tassi & Vizzari, 2020). GEE was chosen because of its broad capabilities in various LULC-based research fields. Midekisa et al. (2017) showed that GEE was able to produce multi-temporal LULC maps on the African continent. Kolli et al. (2020) demonstrated the ability of GEE in analyzing the rate of land use change around Lake Kolleru, India by utilizing the RF algorithm and obtaining an Overall Accuracy (OA) of 95.9 with a Kappa Coefficient (k) of 0.94. Rahman et al. (2020) also analyzed the performance of the RF and SVM algorithms for the urban area of Bhola and the rural area of Dhaka in Bangladesh with an accuracy of 96.9% and 98.3%, respectively. The application of GEE has also reached agricultural areas for crop mapping (Shelestov et al., 2017), comparative analysis of algorithms, and multi-temporal data sets over a wider area (Aguilar et al., 2018). Despite its advantages, in some cases, CART often experiences overfitting when the model fits the training data but fails to generalize the invisible test data

(Lawrence & Wright, 2001). RF tends to require more time in executing data sets to obtain a low Redistribution Error Rate (Prajwala, 2015). Whereas SVM is limited by the number of data sets (Rudrapal & Subhedar, 2015) and class targets. In general, GEE often focuses on climate change, LULC change analysis, and monitoring of water resources with time series analysis (Wang et al., 2018; Workie & Debella, 2018; Jamei et al., 2019). However, GEE has computational limitations in terms of time, storage and memory. Tamiminia et al. (2020) describe these limitations in terms of large computing and memory capabilities; considering the time constraints involved, it is better to use a batch system.

The rapid increase in demand for LULC data and wide area coverage. An understanding of the methods and performance of machine learning that has been widely used, such as GEE is required. The purpose of this study is to classify LULC from the Landsat-8 and Sentinel-2 multispectral satellites, compare the ML algorithm on the GEE platform and compare training data and testing data for the Landsat-8 and Sentinel-2 multispectral satellites to produce a classification with the highest accuracy.

## 2 MATERIALS AND METHODOLOGY

### 2.1 Study Area

The Wanggu watershed is a priority watershed in Southeast Sulawesi Province because of its strategic location, namely, in the upstream part there are forest areas, ex-transmigration of Java, West Java, and Bali as well as spontaneous transmigration (transmigration carried out by local communities themselves).

This area spans an area of 453.44 km<sup>2</sup> based on the UTM 51S projection. This watershed has a strategic function and role because it flows through Kendari City, downstream, and is the center of government, education and economy, industrial area, and clean water source.

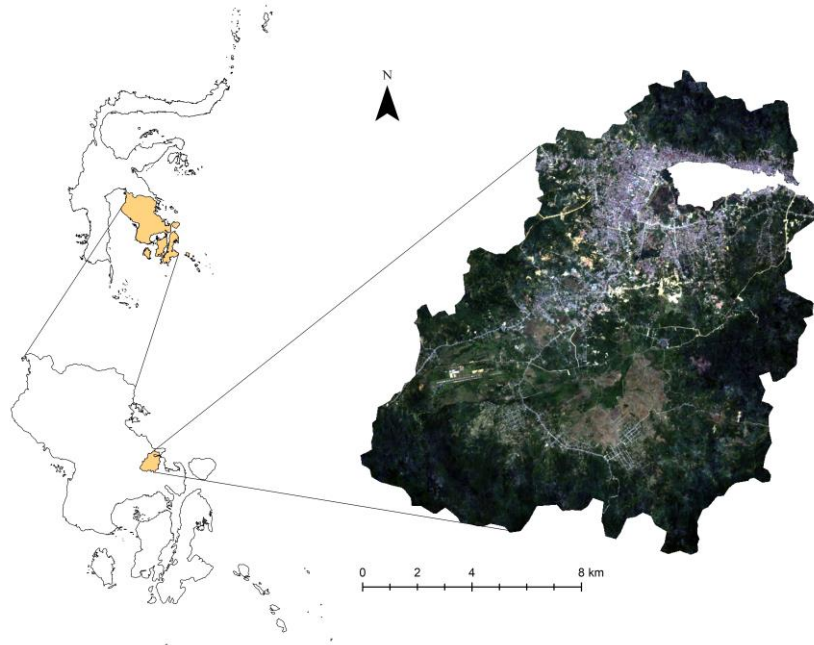


Figure 2-1: Location of map the Wanggu Watershed, Sulawesi Tenggara, Indonesia

**2.2 Data**

Earth Observation Data (EOD) includes satellite imagery from popular platforms such as Landsat and Sentinel stored on GEE's cloud-based platform. Landsat and Sentinel data can be accessed via USGS (The United States Geological Survey) at GEE. This study uses Landsat-8 surface reflectance Tier 1 data which is atmospherically corrected using LASRC (Landsat-8 Surface Reflectance Code) and Sentinel-2 level 1C data. The use of this data is due to constraints such as cloud cover.

Each data is selected with a cloud cover criterion of <10% for each year and the images are combined into a single image. Six Bands (Bands 2-7) of Landsat-8 with 30 m resolution and Nine Bands (Bands 2-8, and 11-12) of Sentinel-2 with 10 m resolution were used in this study (Table 2-1). The LULC class is divided into five main classes: forest, water body, built area, open land, and vegetation. Agricultural and plantation areas are considered vegetation, while rivers and ponds are considered bodies of water.

Table 2-1: Landsat-8 and Sentinel-2 band information

Imagery Data Layer	Source	Band Used	Central Wavelength (µm)	Band Width (µm)	Spatial Resolution (m)
Landsat-8 Operational Land Imager surface reflectance Tier 1	Google Earth Engine (GEE)	Blue (Band 2)	0.482	0.060	30
		Green (Band 3)	0.561	0.067	30
		Red (Band 4)	0.655	0.038	30
		Near-Infra-Red (Band 5)	0.865	0.028	30
		Short-Wave Infra-Red 1 (Band 6)	1.609	0.085	30
		Short-Wave Infra-Red 2 (Band 7)	2.200	0.186	30
		Sentinel-2 MSI: MultiSpectral Instrument, Level-1C	Google Earth Engine (GEE)	Blue (Band 2)	0.496
Green (Band 3)	0.560			0.036	10
Red (Band 4)	0.664			0.031	10
Red-Edge 1 (Band 5)	0.704			0.015	20
Red-Edge 2 (Band 6)	0.740			0.015	20
		Red-Edge 3 (Band 7)	0.782	0.020	20

Near-Infra-Red (Band 8)	0.835	0.106	10
Short-Wave Infra-Red 1 (Band 11)	1.610	0.091	20
Short-Wave Infra-Red 2 (Band 12)	2.202	0.175	20

The Orthorectified image with the least amount of initial cover serves as the main input for classification. After importing satellite data into GEE, the next step is to remove cloud shadows and cloud cover either because it is cloudy or without data using cloud masking (Mateo-García et al., 2018). This technique is suggested and can be optimally performed by GEE (Zurqani et al., 2018; Aldiansyah et al., 2021).

The next satellite image in Composites every year becomes one image using a median filter. The median value is assigned to each pixel in all

images and results in one image for the entire image collection. Each ML algorithm uses 50-75 training data. Each training data is placed on the appropriate land cover type according to the interpretation of image data that has gone through the median filter composite. The generated training data is then split randomly into training data and testing data using predetermined ratios for each LULC map. The LULC training data uses a total of 899 and 802 feature points, respectively on Landsat-8 and Sentinel-2 images.

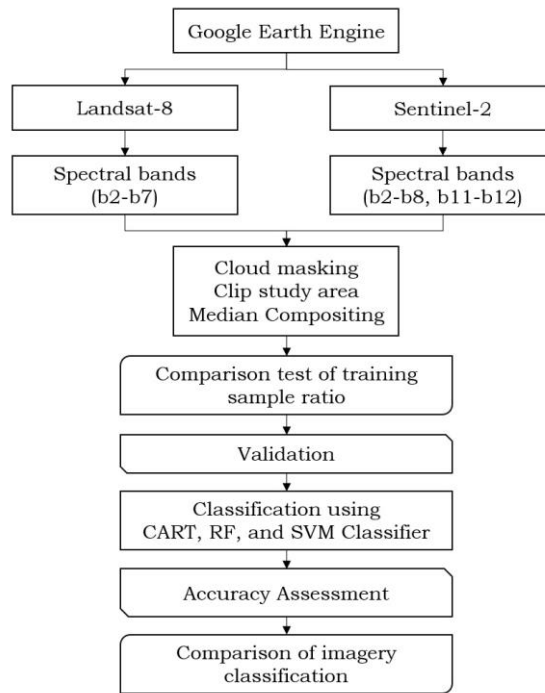


Figure 2-2: Research Flowchat

**2.3 Algorithms**  
**Classification and Regression Tree (CART)**

CART is a binary decision regression tree developed by Breiman et al. (2017) and used for simple decision-making in logical if-then scenarios. CART works recursively by separating nodes until they reach a terminal node, based on a predetermined threshold. The "classifier.smileCart" technique in the

GEE library is used in this study to perform CART classification.

**Random Forest Classifier (RF)**

RF is one of the most commonly used classifiers in constructing an ensemble classification (Brieman, 2001) by combining many CART trees. Several decision trees are generated by RF randomly from training data sets and variables. The optimal number of

calculated trees ranges from 100-500, and the optimal number of variables calculated is the square of the set of variables (Belgiu & Drăguț, 2016). The "classifier.RandomForest" technique in the GEE library is used in this study to classify RF.

### Support Vector Machine (SVM)

SVM is one of the Supervised Machine Learning algorithms used to solve regression and classification problems. The SVM classifier works by creating an ideal hyperplane in the training phase to group multiple classes with inaccurate pixels. The extreme points/vectors are selected to build the hyperplane. This extreme point is called the support vector. Parameters Cost, Gamma, and Kernel function (Adelabu et al., 2015) is used in this study. The cost value used is 10. A higher cost value indicates less incorrect data in the classification. The Gamma value used is 0.5, while the type of Kernel used is Radial or RBF. The "classifier.libsvm" technique in the GEE library is used in this study to classify SVM.

### 2.4 Accuracy Assessment

Assessment of accuracy on the dataset using training data grouping and data testing. A search was conducted on the comparison of datasets to find a good level of accuracy in classifying images. The ratio of accuracy tested is 50:50, 60:40, 70:30, and 80:20. The confusion matrix is used to validate and evaluate the accuracy of image classification. Overall Accuracy (OA) and Coefficient Kappa (k) were also used to test the accuracy of the classification results. The OA and k are calculated from the following equations:

$$OA = \left( \frac{Pc}{Pn} \right) * 100 \quad (2.1)$$

where  $Pc$  is the number of pixels classified correctly and  $Pn$  is the total number of pixels.

$$k = \frac{N \sum_{i=1}^r x_{ii} - \sum_{i=1}^r (x_{i+} * x_{+i})}{N^2 - \sum_{i=1}^r (x_{i+} * x_{+i})} \quad (2.2)$$

where  $r$  = the number of rows and columns in the error matrix,  $x_{ii}$  = the number of observation in row  $i$  and column  $i$ ,  $x_{i+}$  = the marginal total of row  $i$ ,  $x_{+i}$  = the marginal total of column  $i$ , and  $N$  = the total number of observation.

User Accuracy (UA) and Producer Accuracy (PA) are also calculated for each LULC class in the Confusion matrix. Validation with UA is determined by the ratio of the correctly categorized pixels in that class to the total number of pixels classified. Similarly, PA is determined by the ratio of properly categorized pixels to the total number of pixels in the reference data in each class. The classifier that has the best performance will be selected for further image classification for Spatio-temporal change analysis

## 3 RESULTS AND DISCUSSION

### 3.1 LULC Classification Using GEE

This study examines the performance of the ML technique in classifying LULC using Landsat-8 surface reflectance Tier 1 data with a resolution of 30 m and Sentinel-2 data with a resolution of 10 m. Figure 3-2 and Figure 3-3 demonstrate ML algorithms such as CART, RF, and SVM in classifying LULC maps for 2016, 2018, and 2020 on the GEE platform. Orthorectified images with minimal cloud cover and pixels that were damaged due to cloudy conditions were removed from all available images using the Cloud Masking algorithm. Gaps in cloudy images are filled using temporal aggregation methods such as median, mean, and minimum/maximum. This study uses the median value for the collection of Landsat-8 and Sentinel-2 images for 1 year.

The results of the study show that for a more accurate classification it is better to use data from MSI Sentinel-2 when compared to Landsat-8. Explanatory factors that make Sentinel-2's performance better are the presence of additional image channels, especially Red-Edge 1 band, and more detailed spatial resolution. Down-sampling the original spatial resolution of Sentinel-2 data had an approximately equal decreasing effect on the classification performance leaving out the Red-Edge

bands. With almost the same band and by reducing the spatial resolution to 20 m, classification using Sentinel-2 performs better than Landsat-8. This can be an alternative if using MSI Sentinel-2 for mapping with critical processing power or limited by storage capacity. Whereas Landsat-8 works well because it relies more on the ability of Band Blue (B2) to classify forests. Similar studies have also reported the power of the Red-Edge 1 band on the classification of plant and tree species (Immitzer et al., 2016) and the prediction of biophysical variables (Korhonen et al., 2017).

Figure 3-2 and Figure 3-3 show that the classification algorithm generalizes most of the vegetation as open land in 2016 for CART. In the SVM algorithm, most of the open land and water bodies were incorrectly classified as vegetation areas in 2016 and 2018. This is because the type of land cover has a reflection that is identical to the vegetation area. Nonetheless, SVM is quite good at classifying built-up areas and vegetation in 2020.

In Figure 3-1 it can be seen that forest land cover classes and vegetated areas tend to change from time to time, followed by an increase in the built-up area in both imagery types. The forest area decreased to 7.99 km<sup>2</sup> and 45.23 km<sup>2</sup> respectively, while the built-up expanded to 35.88 km<sup>2</sup> in 2020. Vegetation land cover tends to increase to 40.62 km<sup>2</sup> and 23.6 km<sup>2</sup> respectively. The open land experienced decline of 12.48 km<sup>2</sup> and 15.07 km<sup>2</sup> respectively, most of which were closed from forest to become built-up. The same thing happened to the land cover of water bodies which continued to shrink until 3.5 km<sup>2</sup> stopped becoming land.

Human activities have been shown to be responsible for driving these changes resulting in landscape changes that negatively impact ecosystem services and human well-being. (Lambin, 1997; Shiferaw et al., 2019). Main drivers of global environmental change, but not limited to, speed of urbanization (Sreenivasulu & Bhaskar, 2010), increase in population (Hassan & Nazem, 2016), other socio-economic

development activities resulting in deforestation (Torbick, 2006), loss of biodiversity (Sala et al., 2000), change to arable agricultural land (Cihlar, 2000, Renschler & Harbor, 2002), and air resources.

### 3.2 Comparison of Classification Performance

The performance of the most commonly used classifier in evaluating the accuracy and effectiveness of all classifiers through Overall Accuracy (OA). This accuracy represents the number of pixel data correctly classified by the classifier algorithm into percentage form. In addition, the Confusion matrix, and UA and PA are also used to measure the class performance of each classifier. The model with the best capability is selected based on OA and k. The performances of the CART, RF, and SVM classifiers are compared in Table 2-2 and Table 2-3 in terms of OA and k with different forms of dataset division.

Exploration of training tests and data testing was carried out on all algorithms in 2016, 2018, and 2020. The comparison of training and testing datasets with a good level of accuracy was 70:30. The average OA on Landsat-8 and Sentinel-2 was 92.09%, and 94.21%, respectively, followed by a ratio of 60:40, 80:20, and 50:50 on Landsat-8, and a ratio of 80:20, 50:50, and 60:40 on Sentinel-2. Another study also showed that the ratio of dataset comparison in the best RF algorithm was 70:30 (Saha et al., 2021; Adelabu et al., 2015).

From Table 2-2 and Table 2-3, it is also seen that the classifier using RF outperforms the classifier with CART and SVM in both types of satellite imagery. In OA, the mean CART, RF, and SVM classifiers were 92.03%, 94.74%, and 83.54% on Landsat-8. Meanwhile, the average OA of the CART, RF, and SVM classifiers was 93.14%, 96.15%, and 93.34% on Sentinel-2. When compared with CART and SVM, the RF classifier shows the highest producer accuracy and user accuracy, as proven by other studies (Shetty, 2019).

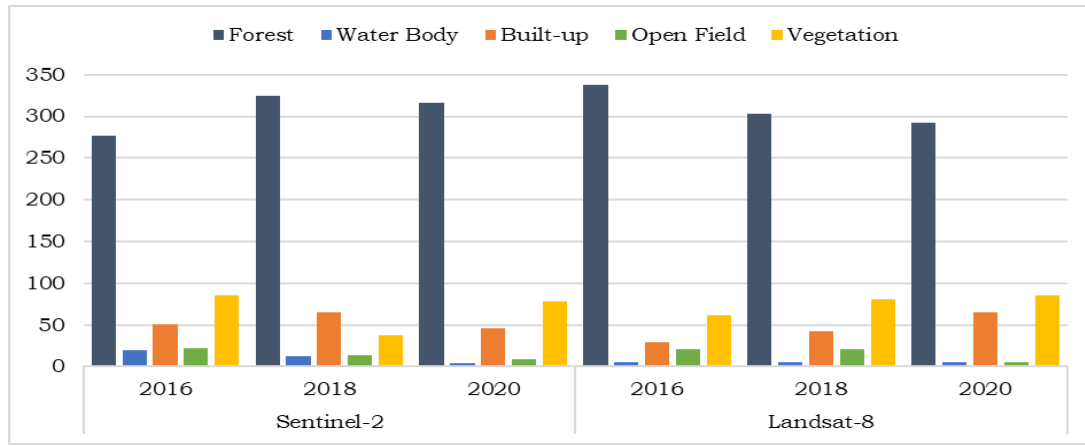


Figure 3-1: LULC changes using RF classifier of Sentinel-2 and Landsat-8 for the years 2016, 2018, and 2020.

Table 2-2: Kappa coefficient and overall accuracy from Landsat-8 for various ratios for comparison of training data and testing data

Year	Classifier	50:50		60:40		70:30		80:20	
		OA (%)	k						
2016	CART	83.33	0.79	89.58	0.86	92.31	0.90	89.36	0.86
	RF	89.17	0.86	93.75	0.91	93.85	0.92	93.62	0.92
	SVM	89.17	0.85	87.5	0.84	87.88	0.84	85.11	0.81
2018	CART	89.47	0.86	88.17	0.84	90.48	0.88	89.13	0.86
	RF	89.47	0.86	93.56	0.92	93.75	0.92	93.49	0.91
	SVM	88.6	0.85	93.55	0.92	93.55	0.92	93.48	0.91
2020	CART	90.91	0.88	93.59	0.92	93.22	0.91	89.74	0.85
	RF	89.9	0.87	93.59	0.92	96.61	0.95	89.74	0.87
	SVM	90.91	0.87	91.03	0.88	87.18	0.79	92.86	0.89

Table 2-3: Kappa coefficient and overall accuracy from Sentinel-2 for various ratios for comparison of training data and testing data

Year	Classifier	50:50		60:40		70:30		80:20	
		OA (%)	k						
2016	CART	83.83	0.73	84.21	0.8	92.54	0.90	90.63	0.87
	RF	90.29	0.79	89.48	0.86	95.59	0.94	93.19	0.91
	SVM	81.81	0.81	89.83	0.79	93.18	0.85	90.48	0.88
2018	CART	93.87	0.88	82.24	0.77	93.23	0.91	93.33	0.91
	RF	97.95	0.93	85.98	0.82	96.05	0.96	96.08	0.92
	SVM	96.47	0.92	91.66	0.85	94.2	0.92	92.04	0.89
2020	CART	87.73	0.77	83.75	0.78	93.65	87.5	92.41	0.9
	RF	92.62	0.91	90	0.87	96.82	0.95	92.45	0.79
	SVM	90.32	0.87	89.41	0.86	92.64	0.85	91.67	0.89

The accuracy of UA and PA in each class is presented in Figure 3-4 and Figure 3-5. It can be seen that compared to other classes, vegetation and water body classes have good performance, with UA and PA above 80%. In contrast to RF, SVM has difficulty identifying water bodies efficiently. This is because

the appearance in the image has very few pixels so it is not enough to train classification accurately and tends to produce poor performance when compared to other land uses. In UA and PA, the SVM classifier mostly performs better than CART on the vegetation class.

It is very difficult to distinguish between vegetation land classes (agriculture/plantation) and open land in the 30 m resolution Landsat-8 imagery because of the mixed pixels. However, this is not a problem with Sentinel-2 imagery. Multiple land use classifications are combined at the same time and allow superior classification for small areas and more land cover types. In this study, the Sentinel-2 image shows a better and clearer image appearance. When compared between Landsat-8 and Sentinel-2, Sentinel-2 produces the highest accuracy results due to the more detailed spatial resolution and the number of band combinations that are applied more than Landsat-8.

Random Forests generally incorporate many soft linear boundaries on the decision surface. In SVM and CART, misclassification occurs between several classes, and SVM works best

when training data is inputted less or less frequently. In this study, when the number of training data inputs is the same as the RF and CART algorithms, the SVM class targets will overlap because each data point exceeds the number of training data specimens that can be processed so that SVM must be run with separate training samples to get optimal results. In line with what was explored by Cervantes et al. (2007), Rudrapal & Subhedar, (2015), and Shetty (2019), that the number of class targets that are too large will also worsen SVM performance, so that in this research the number of suitable classes explored by SVM is 5 classes. Whereas CART and RF classifier do not show significant changes in accuracy if the number of training samples is reduced (Deng & Wu, 2013). This may be a better option if there are less data available (Shetty, 2019).

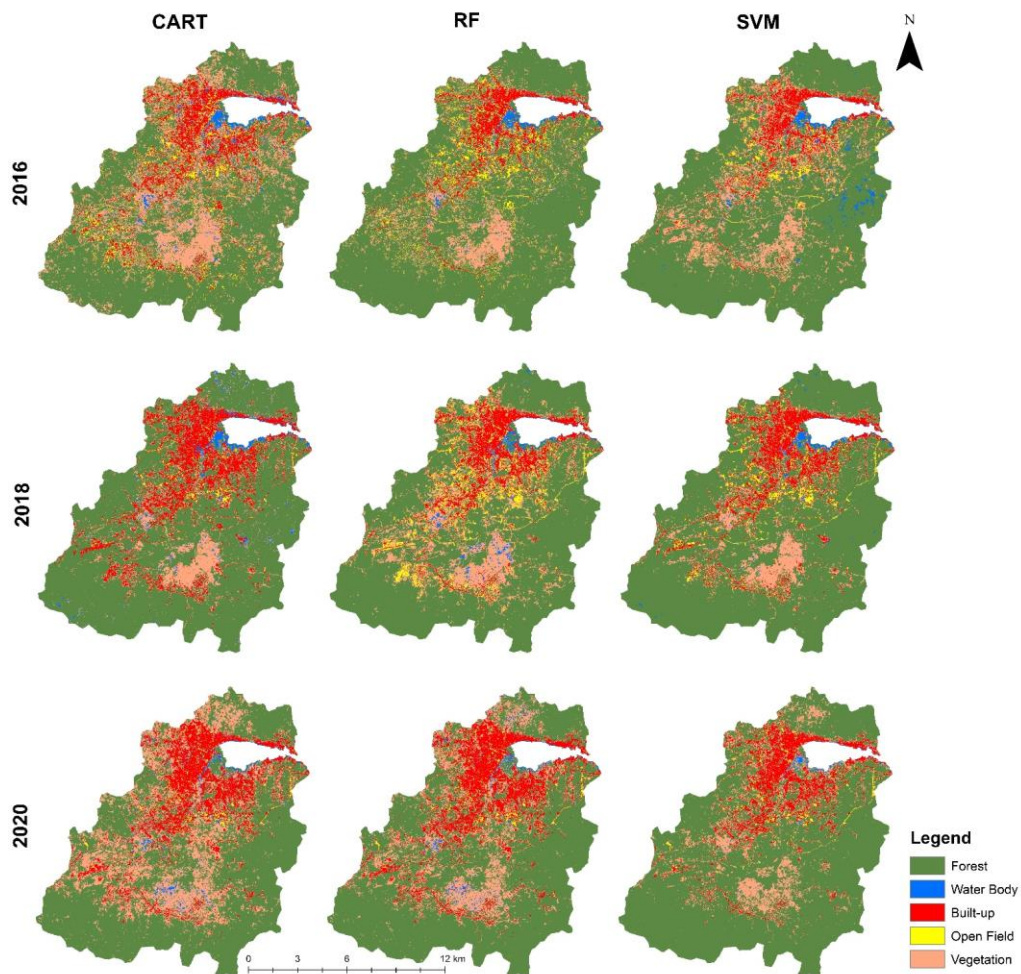


Figure 3-2: LULC Maps from Landsat-8 Imagery with CART, RF, and SVM algorithms for 2014, 2018, and 2021

Each algorithm has advantages and disadvantages. RF is more resistant and less affected by the presence of parameters, whereas SVM is more sensitive to hyperparameters (Chang et al., 2019). In this study, RF did outperform all classifier algorithms in terms of UA and PA, regardless of training data size, followed by CART, then SVM. However, the SVM and CART classifiers performed better for water bodies and forest land cover. Vegetated land cover was partially misclassified as forest by the SVM and CART classifiers. Some studies claim that SVM

outperforms CART (Shao & Lunetta, 2012) or vice versa (Congalton & Green, 2019). In such study, as suggested by Congalton & Green (2019) it is best to choose lesser complex and faster algorithm of the two for classification. The better performance of CART over SVM could be favoured due to the quality of training samples used. The use of multispectral images in GEE can simplify the process of classifying large study areas. This can make performance during image pre-processing more efficient with these implemented methods and algorithms.

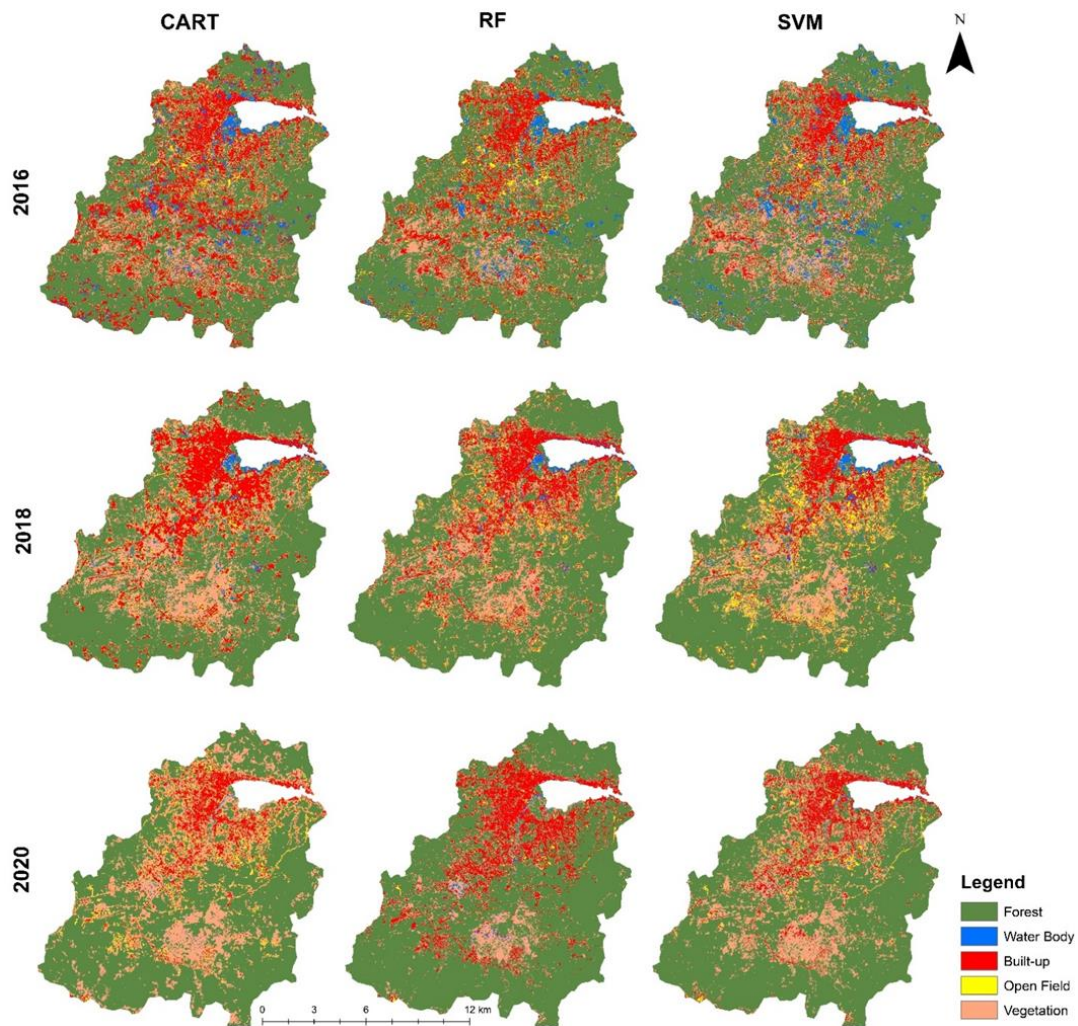


Figure 3-3: LULC Maps from Sentinel-2 Imagery with CART, RF, and SVM algorithms for 2014, 2018, and 2021

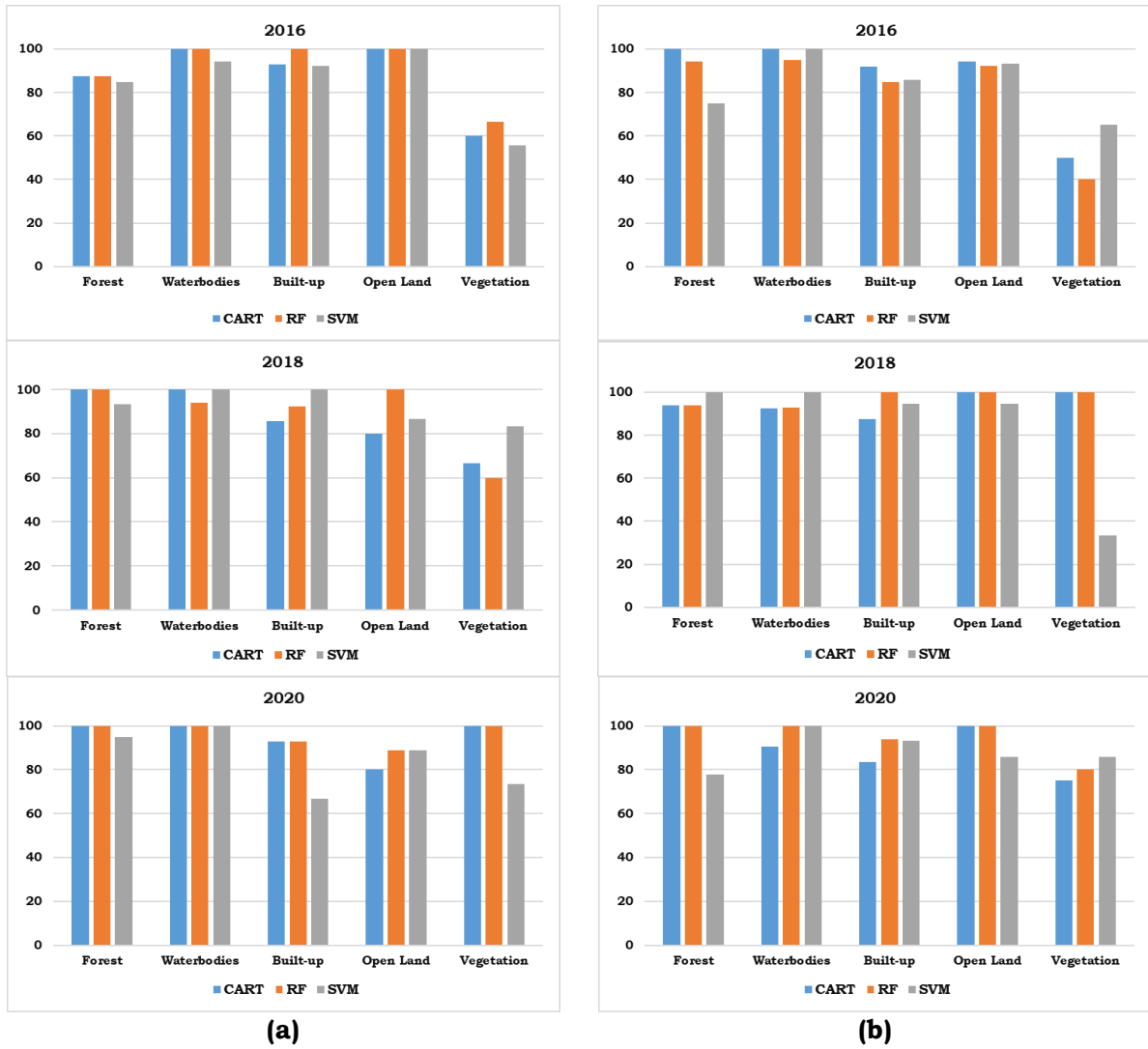
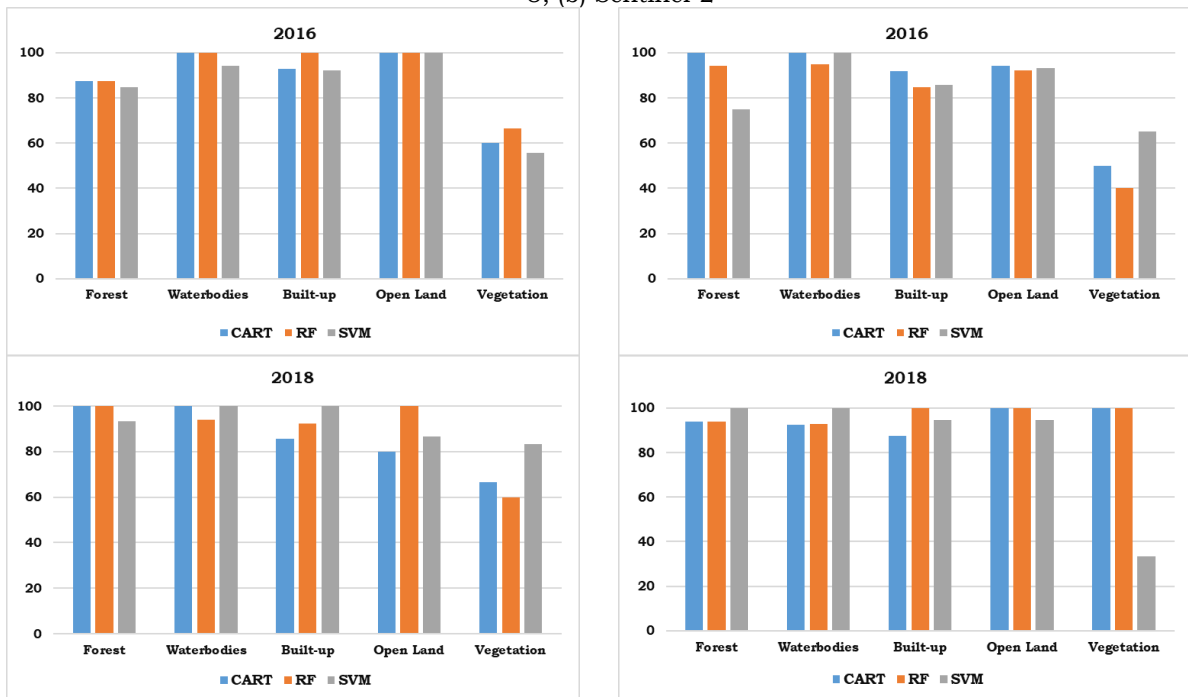


Figure 3-4: Accuracy of the user for each land class using CART, RF, and SVM classifiers: (a) Landsat-8, (b) Sentinel-2



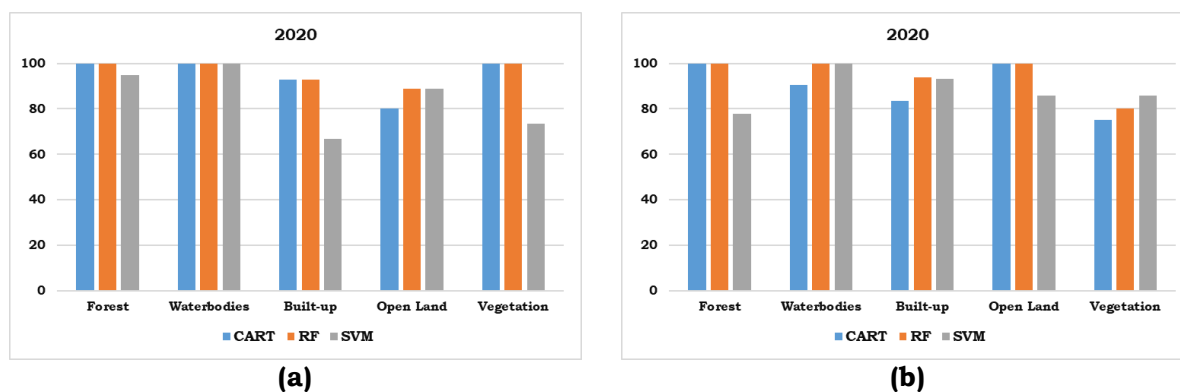


Figure 3-5: Accuracy of the producer for each land class using CART, RF, and SVM classifiers: (a) Landsat-8, (b) Sentinel-2.

#### 4 CONCLUSION

The type of classifier affects the accuracy of the classification of LULC data on satellite images. The comparison between training data and testing data is good at 70:30 for both types of satellite imagery. Overall Accuracy and Coefficient Kappa RF classifier outperforms CART and SVM on both types of satellite imagery. Sentinel-2 imagery performs better classification than Landsat-8 because Sentinel imagery has red-edge bands, which makes it possible to classify vegetation better than Landsat. The high-resolution pixel size also makes Sentinel-2 outperform Landsat-8 in terms of accuracy.

#### ACKNOWLEDGEMENTS

We would like to thank the University of Indonesia for facilitating this research.

#### AUTHOR CONTRIBUTIONS

Author contributions are as follows: Septianto Aldiansyah: imagery processing, conceptualization, methodology, results analysis, map layouting. Randi Andrian Saputra: imagery processing, results analysis, prepare draft manuscript.

#### REFERENCES

Adelabu, S., Mutanga, O., & Adam, E. (2015). Testing the reliability and stability of the internal accuracy assessment of random forest for classifying tree defoliation levels using different validation methods.

Geocarto International, 30(7), 810-821.

- Aguilar, R., Zurita-Milla, R., Izquierdo-Verdiguier, E., & A. de By, R. (2018). A cloud-based multi-temporal ensemble classifier to map smallholder farming systems. *Remote Sensing*, 10(5), 729.
- Aldiansyah, S., Mandini Mannesa, M., & Supriatna, S. (2021). Monitoring of Vegetation Cover Changes with Geomorphological Forms using Google Earth Engine in Kendari City. *Jurnal Geografi Gea*, 21(2), 159-170.
- Bar, S., Parida, B. R., & Pandey, A. C. (2020). Landsat-8 and Sentinel-2 based Forest fire burn area mapping using machine learning algorithms on GEE cloud platform over Uttarakhand, Western Himalaya. *Remote Sensing Applications: Society and Environment*, 18, 100324.
- Belgiu, M., & Drăguț, L. (2016). Random forest in remote sensing: A review of applications and future directions. *ISPRS Journal of Photogrammetry and Remote Sensing*, 114, 24-31.
- Breiman, L. (2001). Random forests. *Machine Learning*, 45(1), 5-32.
- Breiman, L., Friedman, J. H., Olshen, R. A., & Stone, C. J. (2017). *Classification and regression trees*. Routledge.
- Cervantes, J., Li, X., & Yu, W. (2007, November). SVM classification for large data sets by considering models of classes distribution. In *2007 Sixth Mexican International Conference on Artificial Intelligence, Special Session (MICAI)* (pp. 51-60). IEEE.

- Chang, K. T., Merghadi, A., Yunus, A. P., Pham, B. T., & Dou, J. (2019). Evaluating scale effects of topographic variables in landslide susceptibility models using GIS-based machine learning techniques. *Scientific Reports*, 9(1), 1-21.
- Cihlar, J. (2000). Land cover mapping of large areas from satellites: status and research priorities. *International Journal of Remote Sensing*, 21(6-7), 1093-1114.
- Congalton, R. G., & Green, K. (2019). *Assessing the accuracy of remotely sensed data: principles and practices*, 3rd ed. Boca Raton, FL: USA, CRC press.
- Deng, C., & Wu, C. (2013). The use of single-date MODIS imagery for estimating large-scale urban impervious surface fraction with spectral mixture analysis and machine learning techniques. *ISPRS Journal of Photogrammetry and Remote Sensing*, 86, 100-110.
- Gorelick, N., Hancher, M., Dixon, M., Ilyushchenko, S., Thau, D., & Moore, R. (2017). Google Earth Engine: Planetary-scale geospatial analysis for everyone. *Remote Sensing of Environment*, 202, 18-27.
- Hassan, M. M., & Nazem, M. N. I. (2016). Examination of land use/land cover changes, urban growth dynamics, and environmental sustainability in Chittagong city, Bangladesh. *Environment, Development and Sustainability*, 18(3), 697-716.
- Immitzer, M., Vuolo, F., & Atzberger, C. (2016). First experience with Sentinel-2 data for crop and tree species classifications in central Europe. *Remote Sensing*, 8(3), 166.
- Jamali, B., Bach, P. M., Cunningham, L., & Deletic, A. (2019). A Cellular Automata fast flood evaluation (CA-ffé) model. *Water Resources Research*, 55(6), 4936-4953.
- Jamei, Y., Rajagopalan, P., & Sun, Q. C. (2019). Time-series dataset on land surface temperature, vegetation, built up areas and other climatic factors in top 20 global cities (2000–2018). *Data in Brief*, 23.
- Kang, H., Sridhar, V., Mills, B. F., Hession, W. C., & Ogejo, J. A. (2019). Economy-wide climate change impacts on green water droughts based on the hydrologic simulations. *Agricultural Systems*, 171, 76-88.
- Kolli, M. K., Opp, C., Karthe, D., & Groll, M. (2020). Mapping of major land-use changes in the Kolleru Lake freshwater ecosystem by using landsat satellite images in google earth engine. *Water*, 12(9), 2493.
- Korhonen, L., Packalen, P., & Rautiainen, M. (2017). Comparison of Sentinel-2 and Landsat 8 in the estimation of boreal forest canopy cover and leaf area index. *Remote Sensing of Environment*, 195, 259-274.
- Lambin, E. F. (1997). Modelling and monitoring land-cover change processes in tropical regions. *Progress in Physical Geography*, 21(3), 375-393.
- Lawrence, R. L., & Wright, A. (2001). Rule-based classification systems using classification and regression tree (CART) analysis. *Photogrammetric Engineering and Remote Sensing*, 67(10), 1137-1142.
- Liu, D., Chen, N., Zhang, X., Wang, C., & Du, W. (2020). Annual large-scale urban land mapping based on Landsat time series in Google Earth Engine and OpenStreetMap data: A case study in the middle Yangtze River basin. *ISPRS Journal of Photogrammetry and Remote Sensing*, 159, 337-351.
- Mateo-García, G., Gómez-Chova, L., Amorós-López, J., Muñoz-Marí, J., & Camps-Valls, G. (2018). Multitemporal cloud masking in the Google Earth Engine. *Remote Sensing*, 10(7), 1079.
- Midekisa, A., Holl, F., Savory, D. J., Andrade-Pacheco, R., Gething, P. W., Bennett, A., & Sturrock, H. J. (2017). Mapping land cover change over continental Africa using Landsat and Google Earth Engine cloud computing. *PloS One*, 12(9), e0184926.

- Phan, T. N., Kuch, V., & Lehnert, L. W. (2020). Land Cover Classification using Google Earth Engine and Random Forest Classifier—The Role of Image Composition. *Remote Sensing*, 12(15), 2411.
- Pimple, U., Simonetti, D., Sitthi, A., Pungkul, S., Leadprathom, K., Skupek, H., ... & Towprayoon, S. (2018). Google earth engine based three decadal landsat imagery analysis for mapping of mangrove forests and its surroundings in the trat province of Thailand. *Journal of Computer and Communications*, 6, 247-264.
- Prajwala, T. R. (2015). A comparative study on decision tree and random forest using R tool. *International Journal of Advanced Research in Computer and Communication Engineering*, 4(1), 196-199.
- Rahman, A., Abdullah, H. M., Tanzir, M. T., Hossain, M. J., Khan, B. M., Miah, M. G., & Islam, I. (2020). Performance of different machine learning algorithms on satellite image classification in rural and urban setup. *Remote Sensing Applications: Society and Environment*, 20, 100410.
- Rahmi, K. I. N., Ali, A., Maghribi, A. A., Aldiansyah, S., & Atiqi, R. (2022). Monitoring of land use land cover change using google earth engine in urban area: Kendari city 2000-2021. In *IOP Conference Series: Earth and Environmental Science* (Vol. 950, No. 1, p. 012081). IOP Publishing.
- Renschler, C. S., & Harbor, J. (2002). Soil erosion assessment tools from point to regional scales—the role of geomorphologists in land management research and implementation. *Geomorphology*, 47(2-4), 189-209.
- Rudrapal, D., & Subhedar, M. (2015). Land cover classification using support vector machine. *International Journal of Engineering Research & Technology*, 4(09), 584-588.
- Saha, S., Roy, J., Pradhan, B., & Hembram, T. K. (2021). Hybrid ensemble machine learning approaches for landslide susceptibility mapping using different sampling ratios at East Sikkim Himalayan, India. *Advances in Space Research*, 68(7), 2819-2840.
- Sala, O. E., Stuart Chapin, F. I. I., Armesto, J. J., Berlow, E., Bloomfield, J., Dirzo, R., ... & Wall, D. H. (2000). Global biodiversity scenarios for the year 2100. *Science*, 287(5459), 1770-1774.
- Setti, S., Maheswaran, R., Radha, D., Sridhar, V., Barik, K. K., & Narasimham, M. L. (2020). Attribution of hydrologic changes in a tropical river basin to rainfall variability and land-use change: Case study from India. *Journal of Hydrologic Engineering*, 25(8), 05020015.
- Shao, Y., & Lunetta, R. S. (2012). Comparison of support vector machine, neural network, and CART algorithms for the land-cover classification using limited training data points. *ISPRS Journal of Photogrammetry and Remote Sensing*, 70, 78-87.
- Shelestov, A., Lavreniuk, M., Kussul, N., Novikov, A., & Skakun, S. (2017). Exploring Google Earth Engine platform for big data processing: Classification of multi-temporal satellite imagery for crop mapping. *Frontiers in Earth Science*, 5, 17.
- Shetty, S. (2019). Analysis of machine learning classifiers for LULC classification on Google Earth engine. Theses. University of Twente.
- Shiferaw, H., Bewket, W., Alamirew, T., Zeleke, G., Teketay, D., Bekele, K., ... & Eckert, S. (2019). Implications of land use/land cover dynamics and Prosopis invasion on ecosystem service values in Afar Region, Ethiopia. *Science of the Total Environment*, 6175, 354-366.
- Sidhu, N., Pebesma, E., & Câmara, G. (2018). Using Google Earth Engine to detect land cover change: Singapore as a use case. *European Journal of Remote Sensing*, 51(1), 486-500.
- Sreenivasulu, V., & Bhaskar, P. U. (2010). Change detection in land use and land cover using remote

- sensing and GIS techniques. *International Journal of Engineering Science and Technology*, 2(12), 7758-7762.
- Sridhar, V., & Anderson, K. A. (2017). Human-induced modifications to land surface fluxes and their implications on water management under past and future climate change conditions. *Agricultural and Forest Meteorology*, 234, 66-79.
- Sridhar, V., Ali, S. A., & Sample, D. J. (2021). Systems Analysis of Coupled Natural and Human Processes in the Mekong River Basin. *Hydrology*, 8(3), 140.
- Sridhar, V., Billah, M. M., & Hildreth, J. W. (2018). Coupled surface and groundwater hydrological modeling in a changing climate. *Groundwater*, 56(4), 618-635.
- Sridhar, V., Kang, H., & Ali, S. A. (2019). Human-induced alterations to land use and climate and their responses for hydrology and water management in the Mekong River Basin. *Water*, 11(6), 1307.
- Sujatha, E. R., & Sridhar, V. (2018). Spatial Prediction of Erosion Risk of a small mountainous watershed using RUSLE: A case-study of the Palar sub-watershed in Kodaikanal, South India. *Water*, 10(11), 1608.
- Tamiminia, H., Salehi, B., Mahdianpari, M., Quackenbush, L., Adeli, S., & Brisco, B. (2020). Google Earth Engine for geo-big data applications: A meta-analysis and systematic review. *ISPRS Journal of Photogrammetry and Remote Sensing*, 164, 152-170.
- Tassi, A., & Vizzari, M. (2020). Object-oriented lulc classification in google earth engine combining snic, glcm, and machine learning algorithms. *Remote Sensing*, 12(22), 3776.
- Torbick, N. M., Qi, J., Roloff, G. J., & Stevenson, R. J. (2006). Investigating impacts of land-use land cover change on wetlands in the Muskegon River Watershed, Michigan, USA. *Wetlands*, 26(4), 1103-1113.
- Wang, C., Jia, M., Chen, N., & Wang, W. (2018). Long-term surface water dynamics analysis based on Landsat imagery and the Google Earth Engine platform: A case study in the middle Yangtze River Basin. *Remote Sensing*, 10(10), 1635.
- Workie, T. G., & Debella, H. J. (2018). Climate change and its effects on vegetation phenology across ecoregions of Ethiopia. *Global Ecology and Conservation*, 13, e00366.
- Xiao, Y., Hao, Q., Zhang, Y., Zhu, Y., Yin, S., Qin, L., & Li, X. (2022). Investigating sources, driving forces and potential health risks of nitrate and fluoride in groundwater of a typical alluvial fan plain. *Science of the Total Environment*, 802, 149909.
- Xiao, Y., Liu, K., Yan, H., Zhou, B., Huang, X., Hao, Q., ... & Yin, S. (2021). Hydrogeochemical constraints on groundwater resource sustainable development in the arid Golmud alluvial fan plain on Tibetan plateau. *Environmental Earth Sciences*, 80(22), 1-17.
- Xiao, Y., Xiao, D., Hao, Q., Liu, K., Wang, R., Huang, X., ... & Zhang, Y. (2021). Accessible phreatic groundwater resources in the central shijiazhuang of north China plain: perspective from the hydrogeochemical constraints. *Frontiers in Environmental Science*, 475.
- Xie, S., Liu, L., Zhang, X., Yang, J., Chen, X., & Gao, Y. (2019). Automatic land-cover mapping using landsat time-series data based on google earth engine. *Remote Sensing*, 11(24), 3023.
- Zurqani, H. A., Post, C. J., Mikhailova, E. A., Schlautman, M. A., & Sharp, J. L. (2018). Geospatial analysis of land use change in the Savannah River Basin using Google Earth Engine. *International Journal of Applied Earth Observation and Geoinformation*, 69, 175-185